PHYSICAL REVIEW B VOLUME 16, NUMBER 10 15 NOVEMBER 1977

# Electrical properties of forsterite, $Mg_2SiO_4$†

F. J. Morin, J. R. Oliver, and R. M. Housley
*Rockwell International/Science Center, Thousand Oaks, California 91360*
(Received 22 March 1977)

In this paper, we describe a model for the electrical properties of forsterite and report the results of dc conductivity measurements made on single crystals of forsterite and analyzed in terms of the model. It is proposed that the thermal band gap is $E_g = 6.4$ eV and that $Fe^{3+}$ is the major electrically active impurity which introduces an acceptor level 3.0 eV above the valence band. It is found that electronic transport is isotropic, extrinsic and due to holes in the valence band, and that it predominates in the $b$ direction at all temperatures of measurement and in the $a$ and $c$ directions above $\sim 1700$ K. At lower temperatures, extrinsic ionic transport, apparently due to magnesium ions and vacancies, predominates in the $a$ and $c$ directions. We find that the ions and vacancies are bound at lower temperatures, possibly to $Fe^{3+}$ or $Al^{3+}$ ions, with a binding energy of $E_b = 1.9$ to 2.3 eV, and that the ionic transport energy is $E_t(a) = 1.0$ and $E_t(c) = 1.3$ eV. We find no evidence for intrinsic transport of either kind up to the limit of the measurements, 1800 K. This last result may have serious consequences for the interpretation of laboratory data on the pressure and temperature dependence of transport processes in olivine as they apply to its behavior in the earth's mantle.

## I. INTRODUCTION

This study of electrical conduction processes in forsterite was initiated in connection with geophysical interests. It is presumed that olivine, $(Mg, Fe)_2SiO_4$, is the most common mineral of the earth's upper mantle. Therefore, an understanding of electrical conduction in olivine versus temperature and pressure is essential to the interpretation of the electrical conductivity profile in the earth, as inferred from its global electromagnetic response to external magnetic field variations. An understanding of the optical properties of olivine is important to the evaluation of radiative heat transfer in the mantle and a model for the ionic transport in olivine may be important to understanding mechanical creep in the mantle.

There is a very real possibility that in olivine some or all of the above properties are determined by minor or trace impurities. Therefore, in order to directly simulate conditions in the mantle *validly*, olivine samples would have to be equilibrated at each temperature and pressure, with a chemical environment appropriate to the mantle, before measurement. This is a formidable undertaking and has never been attempted.

An alternative and complementary approach which we have adopted is to attempt to identify and separately study the fundamental processes that give rise to optical absorption, ionic transport, and electrical conductivity. Accordingly, our plan has been to begin with the purest available synthetic single-crystal forsterite and to move on to doped single crystals and to natural olivine crystals.

In this paper we describe a model for the electrical properties of forsterite constructed from information in the literature. We also report the results of dc electrical conductivity measurements made on single-crystal forsterite under oxidizing conditions and analyzed in terms of the model. In papers to follow, we plan to report on the results obtained under reducing conditions and on the ac electrical properties of forsterite and on the ac and dc electrical properties of olivine.

## II. AN ELECTRICAL MODEL FOR FORSTERITE

### A. Introductory remarks

In this section we shall review information from the literature in order to construct a model which describes the electrical properties of forsterite. It will be shown that, in many respects, the electrical and optical properties of MgO are similar to those of forsterite. Therefore, the much larger literature on MgO is also used in deriving the model.

MgO is NaCl cubic, $a = 4.21$ Å.[1] The $Mg^{2+}$ ions occupy oxygen octahedra which share edges. Therefore, one expects electronic transport to be isotropic by electrons in the $Mg^{2+}(3s)$ band and holes in the $O^{2-}$ $(2p)$ band. Ionic transport due to magnesium vacancies will also be isotropic.

Forsterite is orthorhombic: $a = 4.77$ Å, $b = 10.195$ Å, $c = 5.981$ Å.[2] As shown in Fig. 1, $Mg^{2+}$ ions occupy two nonequivalent sites, $M_1$ and $M_2$, in oxygen octahedra. Silicon occupies oxygen tetrahedra. The oxygen lattice is very close to the ideal hexagonal close packed. Thus, one expects isotropic-hole transport in the oxygen $(2p)$ band. Continuous rows of $Mg^{2+}$ ions occur only in $M_1$ sites along the $c$ direction in oxygen octahedra which share edges

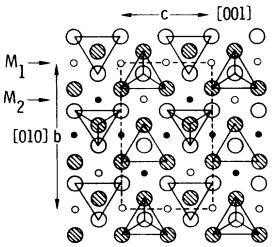


FIG. 1. Forsterite structure parallel to the (100) plane. Si atoms are not shown. Small open circles are Mg ions at $a=0$; small solid circles are Mg ions at $a=\frac{1}{2}$.

and with a Mg-Mg distance of 2.99 Å as in MgO. Since the lowest-lying conduction band is expected to be due to $Mg^{2+}(3s)$ wave functions, it is only in the *c* direction that electron transport in this band may occur. The conduction band due to $SiO_4$ tetrahedral covalent bonds will occur in the *a* and *b* directions, and as shown in Sec. II B, probably lies above the $Mg^{2+}$ $(3s)$ band. Thus, electron transport is probably very anisotropic, being greater along the *c* direction than along the *a* and *b* directions.

Because of the large band gap in forsterite, any measurable amount of electronic transport is expected to be extrinsic. Therefore, we have attempted to provide a detailed diagram of the energy levels introduced into the band gap by chemical impurities and lattice defects. The consequences of these results for electronic transport will be discussed below.

The work of Pluschkell and Engell[3] suggests that ionic transport in nearly stoichiometric forsterite involves magnesium ions but not oxygen ions. Furthermore, the work of Narayan and Washburn[4] on MgO indicates that the energy for production and transport of oxygen vacancies is much greater than that for magnesium vacancies. Hence, in this paper we shall ignore the possibility of oxygen transport and consider only transport due to magnesium ions.

### B. Band gap of MgO and forsterite

The band gap of forsterite is in doubt. In this section we make a tentative decision as to the band gap by comparing Shankland's[5] reflectivity measurements on forsterite with reflectivity for the component oxides MgO and $SiO_2$.

Mg is surrounded by an octahedron of oxygen in MgO and in forsterite. The Mg-O distance is the same in both oxides, the Mg-O bond is essentially ionic, and therefore we can expect energy bands composed of $O^{2-}$ $(2p)$ and $Mg^{2+}$ $(3s)$ and occurring at about the same energy separation in the two oxides. However, as pointed out in Sec. II A, although the valence bands are expected to be isotropic, the $Mg^{2+}$ $(3s)$ conduction band may be lowest lying only in the *c* direction.

Si is surrounded by a tetrahedron of oxygen in $SiO_2$ and in forsterite. The Si-O distance is 0.04 Å greater in forsterite, the bond is essentially covalent, and therefore we can describe the energy bands associated with the $SiO_4$ clusters as forming $sp\sigma$ (bonding) and $sp\sigma^*$ (antibonding) molecular orbitals which occur with slightly less energy separation in forsterite than in $SiO_2$.

The reflectivity of MgO has been measured and analyzed by Roessler and Walker.[6] It consists of two sharp exciton peaks plus rounded peaks from band-to-band transitions which depend upon the joint density of states of the valence and conduction bands. When the exciton peaks are subtracted from the plot of imaginary dielectric constant versus incident photon energy, the band gap of MgO is found to be 7.7 eV.

The reflectivity of $SiO_2$ has been measured by Philipp.[7] It also has a sharp peak suggesting an exciton plus rounded peaks from band-to-band transitions. We have subtracted the assumed exciton peak from the plot of imaginary dielectric constant versus incident photon energy and found the band gap for $SiO_2$ to be about 10.7 eV.

The reflectivity of forsterite shows a rounded peak at 8.4 eV with a shoulder at 7.7 eV. No sharp excitonic peaks are observed. The results suggest that the band gap in forsterite comes at 7.7 eV and that the peak at 8.4 eV is due to the joint density of states of the valence and conduction bands. This value for the band gap agrees well with that for MgO. It also agrees with transmission spectra obtained by Shankland[8] which shows a cutoff between 7.5 and 8.0 eV. Bond-order and bond-energy considerations[9] allow us to take into account the difference in the Si-O distance in $SiO_2$ and forsterite and to estimate the $sp\sigma$-$sp\sigma^*$ separation to be 9 eV in forsterite as compared to 10.7 eV in $SiO_2$. This estimate predicts a peak in the forsterite joint density of states and the reflectivity to occur at ~8.4 eV, in agreement with observation.

We show in Sec. II C that the difference between optical and thermal excitation in MgO is 1.3 eV. Thus, we take the thermal band gap for MgO and forsterite to be 1.3 eV less than the optical band gap or 6.4 eV.

### C. Point-defect energy levels in the band gap of MgO and forsterite

Electrical and optical measurements on appropriately prepared MgO samples allow us to infer the electronic energy levels associated with magnesium and oxygen vacancies and iron, sodium, and hydrogen impurities. Similar measurements on forsterite allow us to determine the levels associated with magnesium vacancies and iron and manganese impurities. The thermal ionization ener-

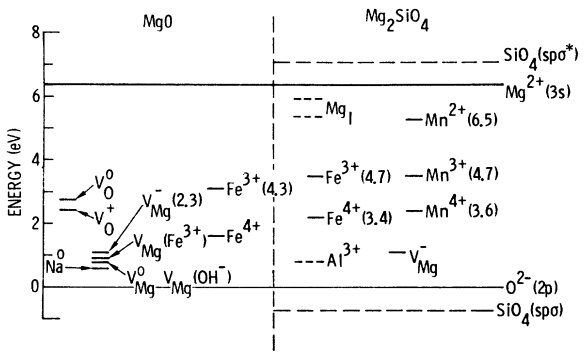


FIG. 2. Energy-level diagram for the band gap of MgO and forsterite together with defect and impurity levels which lie in the band gap.

gies for these levels (optical energy in parentheses) have been summarized in Fig. 2. The thermal-energy information will be used later to explain electronic transport measurements. These energy-level data now will be discussed in some detail.

### *1. Aluminum*

Aluminum is a common impurity in forsterite and olivine. In conformity with its behavior in a number of minerals we assume that it substitutes for Si on tetrahedral sites. Then by analogy with results in quartz[10] we expect it to produce a hole trap slightly above the valence band as shown in Fig. 2.

### *2. Magnesium interstitial*

Magnesium interstitials appear to be a very probable defect in forsterite. Since electronic levels associated with them have not been identified, we tentatively assume that they lie just below the conduction band as shown in Fig. 2.

### *3. Oxygen vacancy*

A set of energy levels for oxygen vacancies is suggested by the considerable amount of work on $F$ centers in MgO. This work indicates that both the $V_0^0$ and the $V_0^+$ centers are located ~5.0 eV (optical) below the conduction band. Kappers *et al.*[11] also show that recombination of electrons in the conduction band with these centers following photoionization produces luminescence bands at 2.4 and 3.0 eV, respectively. We may take the mean of the absorption and emission energies to be the thermal energies for these centers, i.e., 3.7 and 4.0 eV, respectively. These energies for the oxygen vacancy are shown in Fig. 2. These results indicate that the difference between an optical and a thermal-ionization energy is 1.3 eV for a neutral center. We used this difference in Sec. II B to estimate the thermal band gap.

### *4. Magnesium vacancy*

Four acceptor or hole-trap levels have been found associated with a magnesium vacancy in MgO. When the Fermi level lies above these levels, they become occupied. Then an ionized isolated magnesium vacancy $V_{Mg}^{2-}$ will contain two electrons and will introduce two energy levels into the band gap near the valence band. One of the negative charges on the vacancy may be compensated by the presence of a substitutional trivalent ion on a magnesium site neighbor to the vacancy. This will produce $V_{Mg}^-(M^{3+})$ which constitutes a single shallow energy level. One of the negative charges on the vacancy may also be compensated by the presence of a proton on a neighboring oxygen. This will produce $V_{Mg}^-(OH^-)$ which also constitutes a single shallow energy level. Holes trapped in these levels following band-gap irradiation have been detected by thermally stimulated current (TSC),[12] optical absorption,[13] and ESR.[14] The deepest of the four levels is the first level of the isolated vacancy which has the form $V_{Mg}^-$ when one hole has been trapped. This hole may be released by 1.1-eV thermal energy[12] or by 2.3-eV optical energy.[15] The thermal energy for this level is plotted in Fig. 2 together with the optical energy shown in parentheses. The trapped hole constitutes a bound polaron, the optical absorption of which has been explained on the basis of lattice distortion[16] which is responsible for the difference (1.2 eV) between the thermal and the optical ionization energy for the level. An energy difference of 1.2 eV has also been found for bound polarons in $SrTiO_3$.[17] This result is essentially the same as that found above for the $E$(optical)–$E$(thermal) of the $V_0$ centers. This information will be used to convert optical charge transfer energy into thermal energy for manganese and iron levels in forsterite.

Three magnesium vacancy levels lie close together in energy and trap a hole to form $V_{Mg}^0$, $V_{Mg}^0(M^{3+})$, and $V_{Mg}^0(OH^-)$. ESR studies show that holes thermally released from these levels are trapped by the $V_{Mg}^{2-}$ to form $V_{Mg}^-$. Thus, it is clear that $V_{Mg}^-$ is the deepest of the four levels. $V_{Mg}(M^{3+})$ appears to decay at ~300 K which is equivalent to a level lying at about 0.9 eV. $V_{Mg}^0$ and $V_{Mg}(OH^-)$ appear to decay at a slightly lower temperature and probably lie ~0.8 eV above the valence band. These results are shown in Fig. 2.

Sodium substituted for magnesium in MgO also produces a shallow hole trap. The trapped hole is thermally released at ~200 K.[18] This is equivalent to a level at ~0.6 eV above the valence band as shown in Fig. 2.

### 5. *Iron and manganese*

In many oxides a transition-metal ion occupies an oxygen octahedron and an electron may be excited from the $t_{1u}$ and $t_{2u}$ nonbonding $2p$ molecular orbitals of the oxygen into the $d$ levels of the central ion, leaving a hole which is shared by the oxygen of the octahedron. In MgO the top of the valence band is composed of the $t_{1u}$ and $t_{2u}$ orbitals and, therefore, allowed optical transitions may occur from the band edge into a substitutional transition-metal ion. If we assume that $2p$ orbitals having this parity make up the top of the valence band in forsterite, then optical transitions will be allowed from the band edge into the $d$ levels of a transition-metal ion substituting for magnesium. We have already determined the energy difference (1.2 eV) between optical and thermal charge transfer in MgO and $SrTiO_3$. Therefore, from optical charge transfer measurements we may determine the thermal energy of the lowest-lying empty levels of iron and manganese with respect to the valence band of MgO and forsterite.

Charge transfer absorption bands have been reported for $Fe^{3+}$ in MgO by Soshea *et al.*[19] and $Fe^{3+}$ and $Mn^{2+}$ in forsterite by Weeks *et al.*[20] These results are plotted in Fig. 2; the thermal energy is obtained by subtracting 1.2 eV from the optical energy (shown in parentheses). These levels represent deep acceptors which become ionized by the charge transfer reactions

$$Fe^{3+} \rightarrow Fe^{2+} + h, \quad Mn^{2+} \rightarrow Mn^{+} + h,$$

which produce holes at the top of the valence band. The Tippens measurements[21] indicate that optical charge transfer into $Fe^{3+}$ and $Mn^{3+}$ in $Al_2O_3$ appears to occur at about the same energy; consequently, we have plotted the level for $Mn^{3+}$ in forsterite at the same energy as that of $Fe^{3+}$. From the experience with iron in $SrTiO_3$,[22] acceptor levels or trapped holes in the form of $Fe^{4+}$ and $Mn^{4+}$ are expected in MgO and forsterite. If we scale the results of Tippens[21] for $Mn^{4+}$ in $Al_2O_3$ to the band gap of forsterite, we can plot a tentative level for $Mn^{4+}$ in forsterite as shown in Fig. 2.

Mollenkopf *et al.*[14] find that when hole-electron pairs are created in MgO containing $Mn^{3+}$ and $Fe^{3+}$, the ESR signal for $Mn^{2+}$ increases and that for $Fe^{3+}$ decreases. Given the electronic configuration of these ions, it is possible for $Fe^{3+}$ to trap a hole and become $Fe^{4+}$, and $Mn^{3+}$ to trap an electron and become $Mn^{2+}$. A similar result is seen in $SrTiO_3$ doped with $Fe^{3+}$ and $Mo^{6+}$: pumping with band-gap light produces $Fe^{4+}$ and $Mo^{5+}$.[22] However, it is also possible for $Fe^{3+}$ and $Mn^{3+}$ to trap electrons while magnesium vacancies trap the holes. Mollenkopf *et al.* also find that what appears to be a hole trap in MgO empties to produce a glow peak at 500 K. TSC measurements[12] also find an unidentified hole trap which begins to empty around 475 K and located 1.6 eV above the valence band. We shall assume that these results indicate the presence of $Fe^{4+}$ and, accordingly, we show an $Fe^{4+}$ level at 1.6 eV in MgO, Fig. 2.

In the experiments of Weeks *et al.*[20] on $Fe^{3+}$ in forsterite, band-gap irradiation results in a reduction in the optical and ESR signal due to $Fe^{3+}$ together with the appearance of two new optical bands at 2.75 and 3.35 eV. These bands appear to thermally anneal away in about the same temperature range as do $V_{Mg}^{-}$ and $Fe^{4+}$ in MgO and we assign the bands, tentatively, to these centers. The 2.75-eV band is probably not due to charge transfer but represents optical excitation of the bound hole.[16] We shall assume, therefore, that the thermal energy for the $V_{Mg}^{-}$ center is the same in MgO and forsterite. The 3.35-eV band is probably due to charge transfer into $Fe^{4+}$. Therefore, we plot $E(Fe^{4+}) = 3.4 - 1.2 = 2.2$ eV for forsterite in Fig. 2.

## D. Electronic transport

The experience with nominally pure and stoichiometric MgO and forsterite suggest that iron is the major, electrically active background impurity found in these materials. It was pointed out above that $Fe^{3+}$ iron substitutes for $Mg^{2+}$ and is charge compensated by magnesium vacancies. These two point defects introduce acceptor levels in the band gap of MgO and forsterite with occupied $V_{Mg}$ levels lying below the $Fe^{3+}$ levels as shown in Fig. 2. Thus, the Fermi level can be expected to lie on the $Fe^{3+}$ levels, approximately at midgap, unless the MgO and forsterite has been intentially doped with a shallow donor or a shallow acceptor impurity.

If we assume that the Fermi level is pinned near midgap by $Fe^{3+}$ acceptor levels, the resulting hole concentration in the valence band is given by the expression

$$h = N_{vb}([Fe^{3+}]/[Fe^{2+}]) \exp(-E_A/kT), \qquad (1)$$

where $h \ll [Fe^{2+}]$, $N_{vb}$ is the density of states in the valence-band edge, and $[Fe^{3+}]/[Fe^{2+}]$ is the ratio of empty to filled acceptor levels lying at energy $E_A$. When $[Fe^{3+}]/[Fe^{2+}] = 1$ and $E_A = \frac{1}{2}E_{gap}$, this expression also approximates the intrinsic carrier concentration. When $E_{gap}/2 = 3.2$ eV, and the density of states in the valence band is given by $N_{vb} = 4.8 \times 10^{21} T^{3/2} m^{-3}$, and carrier mobility is assumed to be a constant $10^{-4}$ $m^2$ $V^{-1}sec^{-1}$, we get curve 1 in Fig. 3 as being representative of intrinsic electronic conductivity in MgO or forsterite. Extrinsic-hole conduction, due to iron acceptors, will

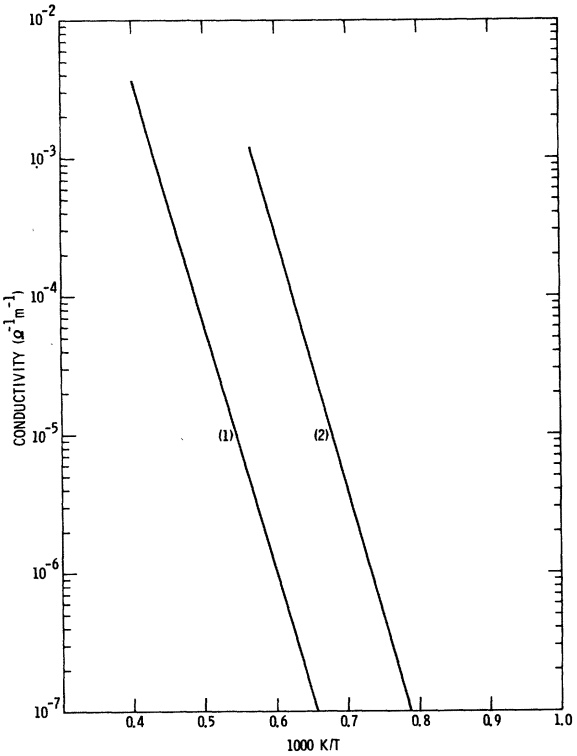


FIG. 3. Electronic conductivity for forsterite (1) calculated intrinsic conductivity; (2) measured, from Ref. 23.

be above curve 1 by the ratio $[Fe^{3+}]/[Fe^{2+}]$.

The only measurement of electronic transport in these materials appears to be that of Mitoff[23] in MgO. From his results on an undoped crystal for which electrical conductivity and the relative fraction of ionic and electronic conductivity was determined we have derived curve 2 in Fig. 3. The slope of this curve is 3.4 eV which is close to that expected for extrinsic transport due to $Fe^{3+}$ acceptor levels. The magnitude of the conductivity suggests a situation for which $[Fe^{3+}]/[Fe^{2+}] \sim 200$.

It is reasonable to assume that the shallow hole traps found in MgO will also occur in forsterite as well as the hole traps introduced by $Al^{3+}$ on Si sites. Thus, a sample which has been thermally quenched or exposed to band-gap illumination may show thermally stimulated conductivity on initial warming.

### E. Ionic transport

Ionic transport along the $c$ direction of forsterite can occur in several ways. Oxygen octahedra which contain the $M_1$ sites share edges in the $c$ direction and all sites are normally occupied. Oxygen octrahedra which contain $M_2$ sites share edges in the $c$ direction with normally empty octahedral sites. One might expect the lower energy transport to occur along the $M_1$ sites if an $M_1$ vacancy is created. This can be an extrinsic vacancy or it can be intrinsic, formed as part of a Frenkel pair by moving an $Mg^{2+}$ from $M_1$ to an empty octahedral site. Transport by $M_1$ vacancies probably requires about the same energy as vacancy motion in MgO. The presence of normally empty octahedral sites suggests a reason for expecting to find that intrinsic transport involves Frenkel defects in forsterite rather than Schottky defects as in MgO.

We must also consider the effect of dislocations and stacking faults on the transport properties. The easy plane for slip is the $a/c$ plane which contains the $M_2$ magnesium sites because in this plane, no Si-O bonds are broken. The easy direction of slip appears to be the $c$ direction which moves hexagonal planes of oxygen ions parallel to one another. Thus, we may expect edge dislocations to occur in the $a$ direction with the possibility of easy ionic transport along the dislocation.

Representative measurements of transport of $Mg^{2+}$ in MgO, forsterite and olivine are plotted in Fig. 4. Where necessary, diffusivity was con-

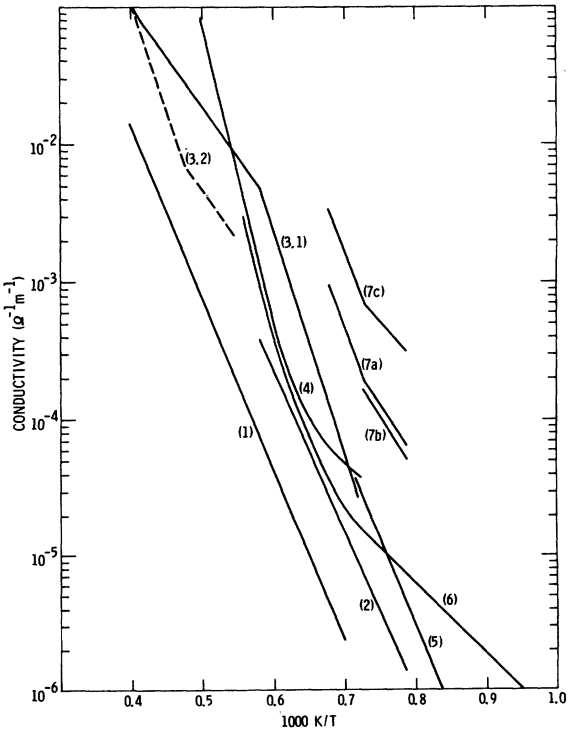


FIG. 4. Ionic conductivity for forsterite curves (4), (5), (6), and (7); and for MgO (1), (2), and (3). Curves (7a), (7b), and (7c) have been plotted a decade higher for clarity.

TABLE I. Ionic transport parameters for MgO and forsterite assuming that electrical conductivity is due to extrinsic magnesium ion vacancy transport. Mg sites in MgO are $5.3\times10^{28}$ $m^{-3}$. Mg sites in forsterite are $2.76\times10^{28}$ $m^{-3}$.

| Sample | $E_t$ (eV) | $n_V$ ($m^{-3}$) | Ref. |
|---|---|---|---|
| MgO | 2.76 | $1\times10^{27}$ | Wuensch *et al.* (Ref. 4) |
| MgO | 2.5 | $1\times10^{27}$ | Mitoff (Ref. 23) |
| Forsterite (*c*) | 2.56 | $6\times10^{27}$ | Misener (Ref. 5) |

verted to conductivity using the Nernst-Einstein relation which gives

$$\sigma = 3.9\times10^{10}D/T\ (\Omega\,\mathrm{m})^{-1} \quad \text{for MgO},$$

$$\sigma = 2.05\times10^{10}D/T\ (\Omega\mathrm{m})^{-1} \quad \text{for forsterite},$$

and $D$ is in $cm^2\,sec^{-1}$.

The most-recent result is curve (1) by Wuensch *et al.*[24] on MgO, which is interpreted by the authors as being extrinsic $Mg^{2+}$ diffusion with an activation energy for migration of 2.76 eV. These results are similar to the ionic component of electrical conductivity of Mitoff[23] curve (2), and diffusion in the *c* direction of forsterite, curve (5) by Misener.[25] If these results are taken to represent the transport energy associated with extrinsic $Mg^{2+}$ vacancy diffusion, the concentration of vacancies $n_V$ may be calculated using the relation

$$\sigma = 1.4\times10^{-20}n_V T^{-1}\exp(-E_t/kT)\ (\Omega\,\mathrm{m})^{-1} \qquad (2)$$

for $n_V$ in $m^{-3}$, where the jump distance is 2.98 Å, the jump frequency given by a 1000-K phonon, and $E_t$ is the energy for transport, omitting small factors such as the number of jump sites available. Table I shows values of $E_t$ obtained from the slope of the curves mentioned above and values of $n_V$ calculated using Eq. (2). We see that in every case the concentration of mobile vacancies is a large fraction of the total $Mg^{2+}$ sites in the crystal, a result not at all consistent with the idea that transport is extrinsic with an activation energy of 2.5 to 2.8 eV.

It has long been known that an adequate interpretation of extrinsic vacancy transport in halides includes an interaction between the vacancy and the aliovalent ion which is compensated by the vacancy, or between the vacancy and impurity precipitates.[26] Harding and Price[27] have taken these factors into account in interpreting their results on the diffusivity of $Mg^{2+}$ in MgO shown in curves (3.1) and (3.2), Fig. 4. The two curves differ in that different amounts of aliovalent impurity were believed to be present in the two experiments. They recognize three regions of behavior: extrinsic vacancy transport with vacancies partially bound to precipitates, having a slope of 3.2 eV from the lower part of curve (3.1); the intermediate region representing transport by vacancies completely free from the bound state, slope 1.56 eV; and intrinsic transport by Schottky defects represented by the upper part of curve (3.2) having a slope of 3.5 eV. From these results the energy of formation of Schottky defects is $E_f = 3.8$ eV, the transport energy for magnesium vacancies is $E_t = 1.56$ eV, and the binding energy between vacancies and binding centers is $E_b = 1.64$ eV. Thus, we see that the slopes of curves (1), (2), and (5) do not represent the transport energy alone. The binding energy of 1.64 eV is larger than that determined by Glass[28] who has measured the binding energy of a $Mg^{2+}$ vacancy to a single aliovalent ion $Cr^{3+}$ in MgO and finds $E_b = 1.08$ eV. This agrees with what one would calculate assuming the binding is due only to Coulombic attraction between $V_{Mg}^{2-}$ and $Cr^{3+}$, that is

$$E_b = 2q^2/\epsilon a = 1.0\ \text{eV} \quad \text{for } \epsilon = 10 \text{ and } a = 2.98\ \text{Å}.$$

The electrical conductivity of forsterite has been measured by Pluschkell and Engell[3] [curve (4)] and Shankland[8] [curve (6)] in Fig. 4. These measurements were on a ceramic and an unoriented crystal, respectively. The low-temperature part of curve (6) extends down to $1/T = 19\times10^{-4}$ $K^{-1}$ with a constant slope of 1.13 eV and appears to represent an extrinsic process. Pluschkell and Engell interpret the upper portion of curve (4) as being intrinsic transport due to the production of $Mg^{2+}$ Frenkel defects.

Buening and Buseck[29] using a fayalite–olivine couple have measured Mg-Fe interdiffusion. Curves (7), Fig. 4 show their results for the case of 10% Fe and $p_{O_2} = 10^{-12}$ atm. In plotting these data the conductivity has been multiplied by a factor of 10 for clarity. The appropriate crystallographic directions are shown by *a*, *b*, and *c*. The same ordering of diffusivity in the three directions has been found by Misener[25] and by Clark and Long[30] on the diffusion of $Ni^{2+}$ in olivine. If we extrapolate the results of Buening and Buseck to forsterite, we find the activation energies for the extrinsic region to be: $E(c) = 1.37$, $E(a) = 1.79$, and $E(b) = 1.85$ eV. The result $E(c) = 1.37$ eV is intermediate between Shankland's result $E = 1.13$ eV and that of Harding and Price for MgO, $E_t = 1.56$ eV, for magnesium vacancy transport.

## III. EXPERIMENTAL

### A. Sample preparation

Boules of synthetic forsterite were obtained from Union Carbide, San Diego. They were about 1×4

cm in size and grown by pulling from the melt in an argon atmosphere. Oriented samples were cut from two boules designated $F1$ and $F2$. The growth direction of $F1$ was along the $a$ direction. That of $F2$ was perpendicular to the $b$ direction and 45° to the $a$ and $c$ directions.

All samples were lapped and polished to a thickness of 0.5–1.0 mm. Concern about the affect of dislocations on the electrical properties led to etching experiments for observation of etch pits. It was found by successive etches in 160 °C phosphoric acid that the samples were damaged to a depth of about 30 $\mu$m by 600 grit wet lapping. However, subsequent measurements showed that this damage had no appreciable affect on the electrical or physical characteristics of the contacts. After the damage had been etched away, it was found that at 100× magnification: no etch pits remained on the $c$ direction samples and the surface was featureless; only a few small clusters of etch pits were seen on the $a$ direction samples and the surface otherwise was featureless: etch pits were numerous on $b$ direction samples from $F1$, whereas samples from $F2$ showed few pits, but a large degree of faceting. After annealing the $b$ direction samples for 24 h in oxygen at 1400 K followed by etching, no appreciable change was seen in the appearance of the surface.

The platinum electrical contacts were fired on at 550 °C in a dry-nitrogen atmosphere using Hanovia liquid-platinum bright. These contacts proved to be satisfactory up to ~1400 K, beyond which a significant loss of contact material began to occur. Sputtered platinum contacts were primarily used for samples measured to higher temperatures since they were found to be more reliable up to 1800 K. The electrical characteristics for both types of contacts were essentially the same, with Ohmic behavior for applied potentials in excess of 100 V/cm. Further evidence of nonblocking contact behavior was obtained in $ac$ experiments to be described in a following paper. Nevertheless, it was found necessary to keep dc fields on the order of 1–20 V/cm in order to limit net ion migration and prevent long-term contact deterioration, particularly at elevated temperatures. Spot checks of the $I$-$V$ characteristics with + and – polarity were taken during the course of the experiments to ensure that the contacts remained Ohmic.

We generally performed experiments on several samples of each crystallographic orientation, and no significant differences between samples from the same boule were observed as long as the conditions of heat treatment were the same. Likewise, the electrical behavior was found to be the same for contacts deposited in different regions on the surface of a given sample. We therefore feel confident that the results presented here truly represent the bulk, and are not influenced by sample nonuniformities which might be present.

### B. Experimental apparatus

All dc and ac measurements were made using the sample holder shown in Fig. 5. The central conductor is shielded by a grounded platinum tube which makes contact with a platinum guard ring on the sample. This arrangement essentially eliminates any measurement errors due to thermionic currents and surface leakage as long as sufficient care is taken to ensure good guard tube alignment and contact preparation. Additional platinum shielding is used on the outer conductors as well, although this is not shown in Fig. 5. The entire holder is enclosed by a high-purity alumina furnace tube, thus enabling complete control of the sample environment. A grounded Pt foil surrounds the outside of the furnace tube in order to reduce ac noise pickup.

Conductivity measurements were made using a Keithley 610C electrometer in conjunction with a

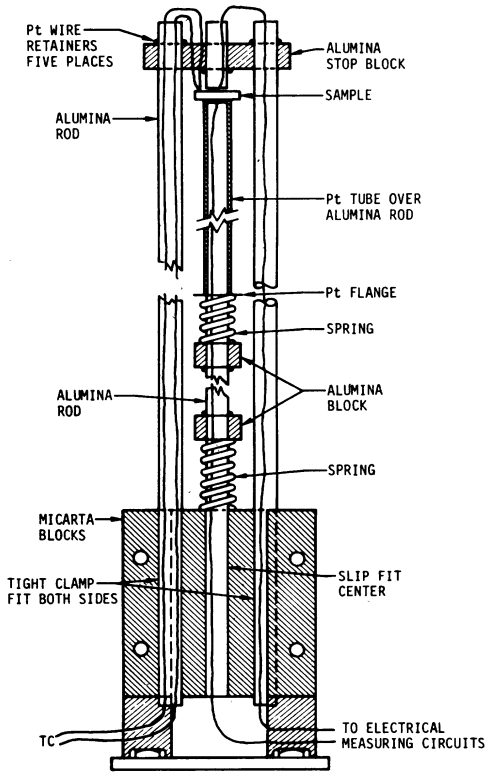


FIG. 5. Schematic drawing of sample holder. The Pt guard tube extends beyond the hot part of the furnace and eliminates currents due to thermionic emission and gas conductivity.

stabilized variable dc voltage supply. The electrometer was operated in the feedback mode so that the guarded low side of the sample was at a virtual ground potential. Additional electronics were used for filtering and logarithmic conversion of the electrometer output, with the log of the sample current recorded continuously versus thermocouple voltage on an $x$-$y$ recorder.

Warming and cooling rates were in the range of 0.1–0.2 K/sec, although they were occasionally slower in instances where deviations from equilibrium became apparent. In general, however, more than one thermal cycle was performed for a given annealing temperature in order to ensure that equilibrium had been achieved.

## IV. EXPERIMENTAL RESULTS

The dc electrical conductivity of forsterite is shown in Figs. 6, 7, and 8. The crystallographic direction of the current flow is designated by *a*, *b*, and *c*. The samples of Figs. 6 and 7 were first equilibrated at 1400 K for about 1 h and then were measured on cooling. The samples of Fig. 8 were equilibrated at 1800 K for about 1 h and measured on cooling. The results were reproducible if the anneal temperature was not exceeded. The *a* and *c* conductivity was not changed significantly at the lower-temperature anneal when the atmosphere was switched from oxygen to nitrogen (containing ~10 ppm oxygen) at atmospheric pressure. The *b* conductivity change was significant, however, and this is shown in Fig. 7. Because the platinum contacts evaporated more rapidly in oxygen, the measurements of Fig. 8 were done in nitrogen.

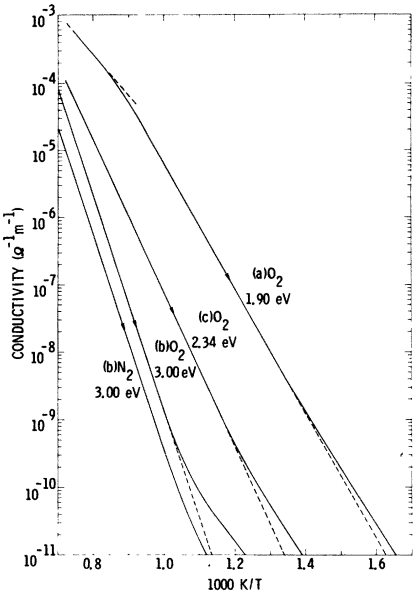


FIG. 7. Measured electrical conductivity of forsterite annealed at 1400 K for the three crystallographic directions, *a*, *b*, and *c*. Samples cut from boule *F*2. Measured in oxygen, *b* remeasured in nitrogen.

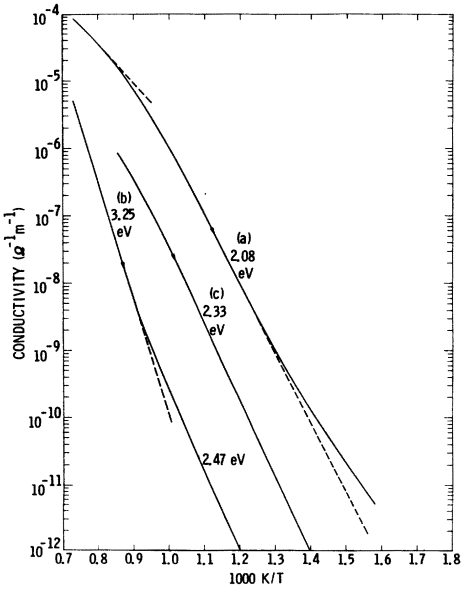


FIG. 6. Measured electrical conductivity of forsterite annealed at 1400 K for the three crystallographic directions *a*, *b*, and *c*. Samples cut from boule *F*1. Measured in nitrogen.

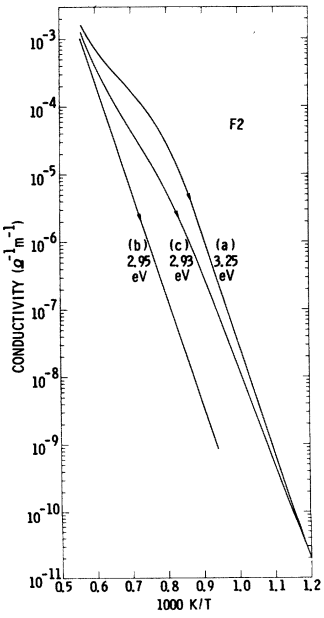


FIG. 8. Measured electrical conductivity of forsterite annealed at 1800 K for three crystallographic directions *a*, *b*, and *c*. Samples cut from boule *F*2. Measured in nitrogen.

The *b* direction shows much lower conductivity than the *a* or *c* direction, but the *a* direction conductivity which diffusion results predicted to be lower than the *c* direction is unexpectedly high. This result is true for both boules and, therefore, is not connected with the growth direction which is different for the two boules. There is the possibility, however, that if dislocations are present, then their most probable orientation is along the *a* direction. Etching experiments on samples from both boules (following removal of all lapping damage) showed a high etch pit concentration on the *a*-*c* plane with very few pits on the *b*-*c* plane and none on the *a*-*b* plane. At present, therefore, we have no explanation to offer for the high conductivity in the *a* direction since we failed to find a large etch pit concentration on the *b*-*c* plane.

The analysis to follow and the ac results to be described in a subsequent paper show that conductivity is electronic in the *b* direction and ionic in the *a* and *c* directions. With this in mind, the activation energies shown in Figs. 6, 7, and 8 are taken from the slopes of the curves corrected for a $T^{3/2}$ term in the case of electronic and a $T^{-1}$ term in the case of ionic conduction.

### A. Electronic transport

The behavior of *ac* conductance and capacitance suggests that transport in the *b* direction is electronic and the positive sign of the thermoelectric effect suggests holes in the valence band. Therefore, the slopes of the *b*-direction curves indicate acceptor levels lying between 3.0 and 3.3 eV above the valence band in accord with predictions of the model which suggests that the most likely acceptor impurity is due to $Fe^{3+}$ levels located near midgap. From a comparison of these results with the curves in Fig. 3 we see that the $[Fe^{3+}]/[Fe^{2+}]$ ratio falls in the region $10^2$ to $10^3$ for the three *b* samples if, indeed, these acceptor levels are due to iron. The results are comparable to Mitoff's result, curve 2, Fig. 3, for MgO. A comparison of the *b* conductivity measured in nitrogen and in oxygen, Fig. 7, serves to support the idea that $Fe^{3+}$ acceptor levels are involved. The slight oxidation achieved by equilibrating in oxygen would be expected to increase the concentration of $Fe^{3+}$ acceptor levels and therefore the conductivity.

### B. Ionic transport

Transport in the *a* and *c* directions is ionic and is assumed to be due to magnesium ions and vacancies. A tail, also due to ionic transport, was sometimes seen in the *b* direction. An example of this is the lower part of curve *b*, Fig. 6. Three temperature regions are prominent in these data: a straight-line region designated by slopes which range between 1.9 and 2.3 eV; a region at higher temperature having a lesser slope; a region where the *a* and *c* conductivity appears to become asymptotic to the *b* conductivity. We note that the decrease in slope at intermediate temperature is similar to the Harding and Price result for MgO. These results suggest that the low-temperature slope is a combination of transport energy and energy of binding between magnesium vacancies and interstitials and aliovalent ions or ion complexes, that the intermediate slope is nearly the transport energy, and that the high-temperature conductivity is a combination of electronic and ionic transport.

For purposes of analysis we take the conductivity to be due to Mg vacancies although a similar discussion could be carried out for extrinsic Mg interstitial conductivity. We may describe the dissociation of an ion-vacancy complex to yield mobile vacancies by the reaction

$$MV \rightleftharpoons M + V .$$

The equilibrium constant for this reaction is given by

$$K = N_M n_V / N_{MV} N_L = \exp(-E_b/kT) ,$$

which includes the equilibrium concentrations of the reactants and $N_L$, the concentration of Mg lattice sites, and $E_b$, the binding energy of the complex. The total concentration of vacancies $N^0_{MV}$, and of aliovalent ions, $N^0_M$ may be expressed as

$$N^0_{MV} = N_{MV} + n_V , \quad N^0_M = N_M + N_{MV} .$$

These equations may be combined to give the following expression for the equilibrium concentration of mobile vacancies:

$$n_V = \tfrac{1}{2}\{-(N^0_M - N^0_{MV} + KN_L) + [(N^0_M - N^0_{MV} + KN_L)^2 + 4KN_L N^0_{MV}]^{1/2}\} . \quad (3)$$

The ionic transport of Figs. 6 and 7 was analyzed in the following steps: (i) the intermediate-temperature slope was taken as a provisional value for the transport energies $E_t(a)$ and $E_t(c)$ using curves (*a*) and (*c*) in Fig. 5 and curve (*a*) in Fig. 7; (ii) with $E_t$ values and Eq. (2), $n_V$-vs-$1/T$ curves were calculated from measured conductivity; (iii) a fit was calculated to these curves using Eq. (3); (iv) from the calculated $n_V$ and the measured conductivity a new estimate of $E_t$ was made and the procedure repeated until the $E_t$ values were self-consistent; and (v) a final small adjustment was made in the $E_t$ values to make the mobile vacancy concentration the same for a given boule in both directions. The resulting curves for $n_V$ are shown in Fig. 9 and the parameters obtained from fitting the curves are shown in Table II.

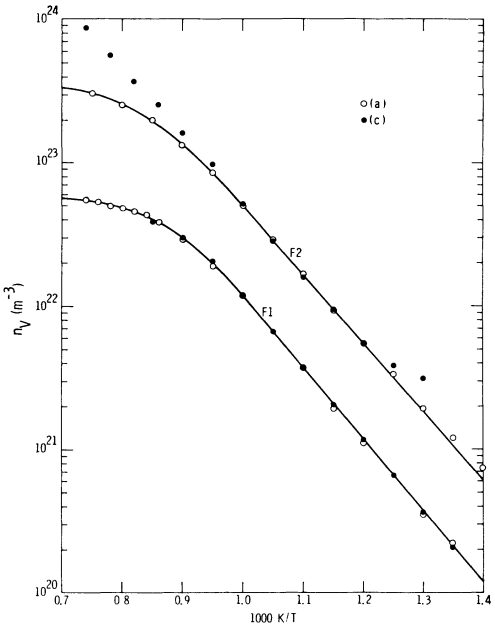


FIG. 9. Mobile vacancy concentration as a function of reciprocal temperature for samples annealed at 1400 K. The points were determined from measured conductivity and calculated mobility using Eq. (2). The solid curves were calculated using Eq. (3) and parameters of Table II.

We note that the number of vacancies equals the number of binding centers in each case. The vacancy concentration in $F2$ is about six times that in $F1$, accounting for the higher conductivity of $F2$. The binding energies and transport energies found for both boules are essentially the same. Since $N^0_{MV} = N^0_M$, the slope is $E_b/2 + E_t$. It was found that a high preexponential factor $e^{\alpha}N_L = 5\times10^{31}$ $m^{-3}$ was required to fit the curves rather than the value $N_L = 5.3\times10^{28}$ $m^{-3}$ magnesium sites. In the preceding analysis, the possible existence of terms such as entropy of transport $S_t$ and the entropy of binding $S_b$ were neglected. (Alternatively, these terms may be considered to be the temperature coefficients of $E_t$ and $E_b$.) If we ascribe the large preexponential factor to these terms, we find that $S_t + S_b = 6.5\times10^{-4}$ eV $K^{-1}$. This result is somewhat larger than that found for MgO by Harding and Price, namely, $S_t + S_b = 2.6\times10^{-4}$ eV $K^{-1}$. In order to separate these terms and to obtain a more reliable value for them, we would require an independent determination of the values for $N^0_{MV}$.

TABLE II. Parameters derived from an analysis of the temperature dependence of the mobile vacancy concentration shown in Fig. 9 for samples annealed at 1400 K.

| Boule | $F1$ | $F2$ |
|---|---|---|
| $E_b$ (eV) | 2.03 | 1.94 |
| $N^0_{MV} = N^0_M$ ($m^{-3}$) | $5.6\times10^{22}$ | $3.5\times10^{23}$ |
| $e^{\alpha}N_L$ ($m^{-3}$) | $5\times10^{31}$ | $5\times10^{31}$ |
| $E_t(a)$ (eV) | 1.04 | 1.00 |
| $E_t(c)$ (eV) | 1.33 | 1.38 |

Curve ($c$) in Fig. 7 contains a significant contribution from the electronic conductivity. We may estimate this contribution by subtracting a calculated ionic conductivity from the measured conductivity. When this is done, we find an electronic conductivity in the $c$ direction to be a factor of 2.5 greater than that found in the $b$ direction but with the same slope. This is not surprising because these samples were not all annealed together and thus did not receive identical treatment. The measurements are not precise enough to be interpreted as meaning that the electronic term is different in the two directions. The electronic conductivity, like the mobile vacancy conductivity, is about six times greater in $F2$ than in $F1$. This result is consistent with the idea that $Fe^{3+}$ impurity is responsible for the holes in the valence band and for the magnesium vacancies.

The binding energies are larger than $E_b = 1.64$ eV found by Harding and Price in MgO and much larger than that expected if a single aliovalent ion is involved. Thus, as suggested by Harding and Price, we may be dealing with a precipitate which contains both the vacancies and aliovalent ions. Harding and Price reported $E_t = 1.56$ eV for MgO. However, in doing this they did not take into account the temperature dependence of $n_V$ as our analysis has done. Therefore, it seems probable that $E_t$ for MgO is fairly close to the value $E_t(c) = 1.33$ eV which we find for forsterite. This lower estimate for $E_t$ results in a higher value for $E_b$ in MgO, also more nearly in agreement with our value for forsterite.

It is interesting that the activation energy $E = 1.13$ eV for conductivity measured by Shankland, curve 6 in Fig. 4 on an unoriented sample lies midway between our values for $E_t(a)$ and $E_t(c)$. Using that value and Eq. (2) we estimate that $n_V = N^0_{MV} = 2\times10^{22}$ $m^{-3}$ for Shankland's sample. There is no evidence that the vacancies are bound in that case, a situation which occurs when $N^0_{MV} > N^0_M$.

The electrical conductivity of samples from boule $F2$ annealed at 1800 K and shown in Fig. 8 was analyzed as described above. The resulting curves of mobile vacancy concentration are shown in Fig. 10 and the parameters derived from fitting these curves are shown in Table III. It was found that the results for the $a$ direction were quite consistent with the previous results. The same values were found for $E_t$ and $e^{\alpha}N_L$. Annealing at the

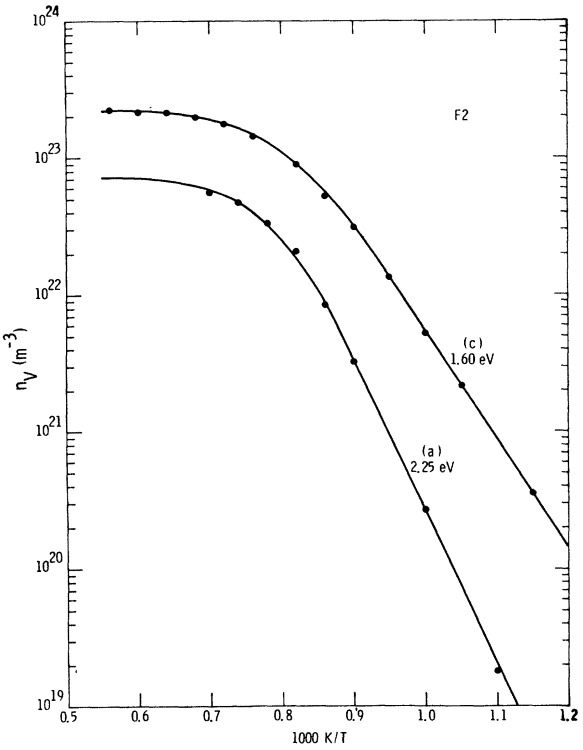


FIG. 10. Mobile vacancy concentration as a function of reciprocal temperature for samples annealed at 1800 K. The points were determined from measured conductivity and calculated mobility using Eq. (2). The solid curves were calculated using Eq. (3) and parameters of Table III.

higher temperature decreased both $N^0_{MV}$ and $N^0_M$. In the high-temperature case, however, $N^0_M > N^0_{MV}$ so that the slope of the $n_V$ curve is $E_b$ rather than $\frac{1}{2}E_b$ and the slope of the conductivity curve is given by $E_t + E_b$. The decrease in both $N^0_{MV}$ and $N^0_M$ is consistent with the expectation that annealing in nitrogen at high temperature would remove oxygen from the lattice, close in the lattice thus reducing the magnesium vacancy concentration, and change the $Fe^{3+}$ to $Fe^{2+}$ which decreases the concentration of aliovalent ions. Annealing increased the binding energy slightly.

TABLE III. Parameters derived from an analysis of the temperature dependence of the mobile vacancy concentration shown in Fig. 10 for boule $F2$ samples annealed at 1800 K.

| Sample | (a) | (c) |
|---|---|---|
| $E_b$ (eV) | 2.25 | 1.60 |
| $N^0_{MV}$ ($m^{-3}$) | $7.2\times10^{23}$ | $2.2\times10^{23}$ |
| $N^0_M$ ($m^{-3}$) | $1.3\times10^{23}$ | $3.6\times10^{24}$ |
| $e^{\alpha}N_L$ ($m^{-3}$) | $5\times10^{31}$ | $1\times10^{31}$ |
| $E_t$ (eV) | 1.00 | 1.33 |

The $n_V$ curve in Fig. 10 for the $c$ direction and the parameters derived from fitting it are not consistent with previous results nor with the results for the $a$ direction. The binding energy appears to have decreased, the value for $N^0_M$ to have increased to an unreasonable number, the preexponential factor required for the fit is different. Although one might expect the values for $N^0_{MV}$ to be different for the $a$ and $c$ samples because treatment and location in the boule was not identical, it cannot be accepted that the binding energy and thus the overall shape of the curves can be different. The $c$ direction results can be made consistent with those of the $a$ direction if it is assumed that there are two transport mechanisms operating in the $c$ direction. This is not unrealistic since there are two magnesium sites and thus energetically quite different paths by which a magnesium may move in the $c$ direction. Thus, we require in addition to a process given by Eq. (2) and $E_t = 1.33$ eV, another process in which the preexponential factor of Eq. (2) is reduced to $3.3\times10^{-23}$ from $1.4\times10^{-20}$ and with $E_t = 0.65$ eV. More work must be done, however, before we can feel confident that this is a real result.

The 1800-K anneal reduced the $b$ direction electronic conductivity by about a factor of 4 from that of the 1400-K treatment, consistent with a decrease in the concentration of $Fe^{3+}$ acceptors, but did not appreciably change the location of the Fermi level. In the analysis of the ionic conductivity of Fig. 8 it was found that the electronic component in the $a$ direction was a factor of 1.5 less than in the $b$ direction. The electronic component in the $c$ direction was found to be the same as in the $b$ direction. Thus, it appears that, within the limits of measurement, the electronic conductivity in the valence band is isotropic as predicted by the model.

The high-temperature measurements of Pluschkell and Engell and of Shankland curves (4) and (6) in Fig. 4 show a rapid increase in conductivity above $1/T = 7\times10^{-4}$ $K^{-1}$. We have found no evidence of this behavior and must conclude that intrinsic ionic conductivity becomes appreciable only at higher temperatures. However, we have observed behavior which was very similar to theirs when we tried to make conductivity measurements with unguarded contacts. The excess current in that case may have been due to thermionic emission from the contacts.

Additional experiments are required to support and extend the results which we have obtained. The study of crystals doped to several different, but known, levels of $Fe^{3+}$ concentration could lead

to establishing the role of $Fe^{3+}$ as an acceptor level in the band gap and possibly a determination of $N_{IV}^0$ which would allow an estimate of the preexponential factor in the expression for ionic conductivity. An independent determination of $[Fe^{3+}]$ and total iron content would yield $[Fe^{3+}]/[Fe^{2+}]$ and an estimate of hole mobility. Analysis of the dependence of conductivity on $p_{O2}$ for suitably doped samples would allow an estimate of the location in the band gap of the oxygen vacancy level.

## V. CONCLUSIONS

We have partially described and analyzed an extensive set of electrical properties data on oriented single-crystal forsterite samples. In order to facilitate the discussion of the data reported and data to be presented subsequently we have developed and described a model for the electronic properties of forsterite including the energy of a number of expected impurity levels.

dc conductivity values differ by more than three orders of magnitude with crystallographic direction in these samples. The conductivity in the most insulating *b* direction has been identified with electronic hole motion. The magnitude and temperature dependence of this conductivity correspond with the predictions of our model for extrinsic holes associated with $Fe^{3+}$ impurities.

The conductivity in the *a* and *c* directions is extrinsic ionic conductivity and has been fitted in detail using a consistent and reasonable set of binding and transport energies.

Thus, all electrical conduction and ionic transport processes observed in our forsterite crystal up to 1800 K are extrinsic. Since our conductivity and ionic transport values are as low as any reported on forsterite all other workers must also have been dealing with extrinsic processes.

Conductivity and ionic transport values obtained on olivine are consistently higher than those obtained on forsterite. Therefore, there is a strong implication that observed transport processes in olivine are also extrinsic in nature.

Such an inference is of fundamental geophysical significance. It calls into question the validity of using any laboratory data to infer the transport properties of olivine in the earth's mantle, *unless* the sample is equilibrated with a chemical environment appropriate to the mantle at each temperature and pressure.

---

†Work partially supported by ONR Contract No. N00014-76-C-0653.

[1]R. W. G. Wycoff, Interscience 1, 185.
[2]H. S. Yoder and T. G. Sakama, Am. Mineral 42, 475 (1957).
[3]W. Pluschkell and H. J. Engell, Ber. Dtsch. Keram. Ges. 45, 388 (1968).
[4]J. Narayan and J. Washburn, Acta Metall. 21, 533 (1973).
[5]T. J. Shankland, Science 161, 51 (1968).
[6]D. M. Roessler and W. C. Walker, Phys. Rev. 159, 733 (1967).
[7]H. R. Philipp, Solid State Commun. 4, 73 (1966).
[8]T. J. Shankland, Office of Naval Research Report No. NR-017-308 (unpublished).
[9]H. S. Johnston and C. Parr, J. Am. Chem. Soc. 85, 254 (1963).
[10]J. A. Weil, Radiat. Eff. 26, 261 (1975).
[11]L. A. Kappers, R. L. Kroes, and E. B. Hensley, Phys. Rev. B 1, 4151 (1970).
[12]W. C. Mallard and J. H. Crawford, J. Appl. Phys. 43, 2060 (1972).
[13]L. A. Kappers, F. Dravneiks, and J. E. Wertz, J. Phys. C 7, 1387 (1974); Solid State Commun. 10, 1265 (1972).
[14]H. C. Mollenkopf, L. E. Halliburton, and E. E. Kohnke, Phys. Status Solidi A 19, 243 (1973); Phys. Rev. Lett. 30, 607 (1973).
[15]B. Henderson and J. E. Wertz, Adv. Phys. 17, 749 (1968).
[16]O. F. Schirmer, P. Koidl, and H. G. Reik, Phys. Status Solidi B 62, 385 (1974).
[17]F. J. Morin and J. R. Oliver (unpublished).
[18]M. M. Abraham *et al.*, Phys. Rev. B 5, 4945 (1972).
[19]R. W. Soshea, A. J. Dekker, and J. P. Sturz, J. Phys. Chem. Solids 5, 23 (1958).
[20]R. A. Weeks, J. L. Pigg, and C. B. Finch, Am. Mineral 59, 1259 (1974).
[21]H. H. Tippens, Phys. Rev. B 1, 126 (1970).
[22]B. W. Faughnan, Phys. Rev. B 4, 3623 (1971).
[23]S. P. Mitoff, J. Chem. Phys. 36, 1383 (1962); 41, 2561 (1964).
[24]B. J. Wuensch, W. C. Steel, and T. Vasilos, J. Chem. Phys. 58, 5258 (1973).
[25]D. J. Misener, *Geochemical Transport and Kinetics*, Publication No. 634, (Carnegie Institute, Washington, D. C., 1973), p. 117.
[26]R. W. Dreyfus and A. S. Nowick, Phys. Rev. 126, 1367 (1962).
[27]B. C. Harding and D. M. Price, Philos. Mag. 26, 253 (1972).
[28]A. M. Glass, J. Chem. Phys. 46, 2080 (1967).
[29]D. K. Buening and P. R. Buseck, J. Geophys. Res. 78, 6852 (1973).
[30]A. M. Clark and J. V. P. Long, *International Thomas Graham Memorial Symposium, 1969*, edited by J. N. Sherwood *et al.* (Gordon and Breach, New York, 1970).